

Artigo

Kinetic Mechanism Study of Reaction $C_2H + C_2H_2$ via TST

da Silva, W. B.;* Albernaz, A. F.

Rev. Virtual Quim., 2016, 8 (2), 394-404. Data de publicação na Web: 15 de março de 2016<http://rvq.sbq.org.br>**Estudo do Mecanismo Cinético da Reação $C_2H + C_2H_2$ via TST**

Resumo: Neste trabalho, apresentamos a Superfície de Energia Potencial da reação-SEP do C_2H com a molécula C_2H_2 . Mais precisamente, determinamos as geometrias, frequências e energias eletrônicas para as diferentes espécies envolvidas nos caminhos de reação do processo $C_2H + C_2H_2$ usando os níveis de cálculo B3LYP/6-311++G(d,p) e CBS-QB3. A partir deste estudo, calculamos a taxa de reação via Teoria da Estrutura de Transição - TST. A reação acontece em dois caminhos e suas taxas de reação foram calculadas para a faixa de temperatura de 100 - 4200K.

Palavras-chave: Superfície de Energia Potencial; C_2H ; C_2H_2 ; Reação $C_2H + C_2H_2$; Taxa de Reação.

Abstract

In this work, we present the Potential Energy Surface – PES of the reaction of C_2H with C_2H_2 molecule. More precisely, we determined the geometries, frequencies, and electronic energies for the species involved in the $C_2H+C_2H_2$ reaction pathways at the B3LYP/6-311++G(d,p) and CBS-QB3 levels. From this study, we calculated the Rate Constant for two pathways of the reaction via Transition State Theory - TST. The reaction proceeds in two steps and rate constants were calculated for the temperature range 100 - 4200K.

Keywords: Potential Energy Surface; C_2H ; C_2H_2 ; $C_2H + C_2H_2$ Reaction; Rate Constant.

* Universidade de Brasília, Instituto de Física, Campus Universitário Darcy Ribeiro, CEP 70910-900, Brasília-DF, Brazil. Instituto Federal de Educação, Ciência e Tecnologia de Goiás, Campus Luziânia, CEP 72811-580, Luziânia-GO, Brazil.

✉ wassestf@gmail.com

DOI: [10.5935/1984-6835.20160029](https://doi.org/10.5935/1984-6835.20160029)

Kinetic Mechanism Study of Reaction $C_2H + C_2H_2$ via TST

Washington B. da Silva,^{a,b,*} Alessandra F. Albernaz^a

^a Universidade de Brasília, Instituto de Física, Campus Universitário Darcy Ribeiro, CEP 70910-900, Brasília-DF, Brazil.

^b Instituto Federal de Educação, Ciência e Tecnologia de Goiás, Campus Luziânia, CEP 72811-580, Luziânia-GO, Brazil.

* wassestf@gmail.com

Recebido em 15 de março de 2016. Aceito para publicação em 15 de março de 2016

1. Introduction

2. Computational Methods

2.1. Ab Initio Calculations

3. Results and Discussion

3.1. Potential Energy Profile and Reaction Mechanism

3.2. Rate Constants

4. Conclusions

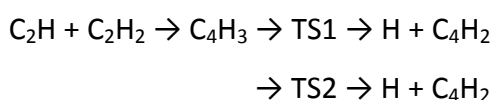
1. Introduction

The neutral-neutral reactions in chemistry of interstellar and circumstellar clouds involving H_2C_2 has been studied in the chemistry of interstellar and circumstellar clouds.¹⁻⁸ Some species like acetylene, H_2C_2 , for instance, has been directly observed in the atmospheres of Jupiter, Saturn, or Titan.^{9,10} A possibly important class of neutral-neutral reactions in interstellar and circumstellar sources consists of so-called condensation reactions between hydrocarbon radicals and neutrals to form more complex species. The prototypical reaction of this sort – and the one best studied in the laboratory¹ is $C_2H + C_2H_2 \rightarrow C_4H_2 + H$. This reaction has been investigated at temperatures of 300 K and above, but the

results cannot easily be extrapolated to below room temperature; indeed, there is a wide divergence of results at 300 K that show that the reaction is quite rapid but do not foreclose on the possibility of a small potential barrier that could eliminate the possibility of reaction at low temperatures.¹ The ethynyl radical, C_2H , is known to be an important intermediate in a number of chemical systems. In combustion it plays a key role in the initial stages of soot formation,¹¹ and it has also been detected in interstellar space¹² and in planetary atmospheres.¹³ In the literature we find experimental researchs such as Laufer and co-workers that studied reactions with O_2 , H_2 , C_2H_2 , and a number of other small hydrocarbons by using flash photolytic production of C_2H .¹⁴⁻¹⁶ The O_2 and C_2H_2 reactions were followed by observing the

appearance of the reaction products CO and C₄H₂, respectively, and the rate of reaction with H₂ was deduced by measuring the dependence of the rate of butadiyne production (arising from the reaction of ethynyl radicals with the acetylene precursor) on the partial pressure of added H₂.²

Given the importance of this reaction in



chemistry of circumstellar sources we decided to study the reaction C₂H + C₂H₂. In this work, we present a new potential energy profile for the C₂H+C₂H₂ reaction at the B3LYP/6-311++G(d,p)¹⁷ and CBS-QB3¹⁸ levels and we calculated rate constants for the pathways. This new finding provides one new pathway for this reaction:

$$(\Delta H_{\text{B3LYP}}^{300\text{K}} = -37.09 \text{ kcal/mol})$$

$$(\Delta H_{\text{CBS-QB3}}^{300\text{K}} = -40.43 \text{ kcal/mol})$$

2. Computational Methods

2.1. Ab Initio Calculations

The hybrid density functional B3LYP and CBS-QB3 methods combined with the 6-311++G(d,p) basis set has been employed in our work to optimize the geometries of the reactant, complex reactants, transition states, complex products and products of the C₂H+C₂H₂ reaction. Vibrational frequencies calculated at B3LYP and CBS-QB3 levels were used for characterization of stationary points as minima and transition states, for zero-point energy (ZPE) corrections, because it is known that the ZPE value is significant in hydrogen-bonded systems.¹⁹ The number of imaginary frequencies (0 or 1) indicates whether a minimum or a transition state has been located. To confirm that the transition state really connects with designated intermediates along the reaction path, the intrinsic reaction coordinate (IRC) calculations were performed. Also, the intrinsic reaction coordinate (IRC)²⁰ calculations were used to confirm the connection between the designated transition states and the reactants or products. All quantum chemistry calculations were performed with Gaussian 09 program.²¹ The relative energies (the total energy of the reactants is set to zero for reference) of all species involved at the B3LYP and CBS-QB3

levels are summarized in Figure 1. The five step CBS-QB3 series of calculations start with a geometry optimization at the B3LYP/6-311G(2d,d,p) level, followed by a frequency calculation to obtain thermal corrections, zero-point vibrational energy, and entropic information.²²

3. Results and Discussion

3.1. Potential Energy Profile and Reaction Mechanism

Figure 1 shows the potential energy profile of the C₂H+C₂H₂ reaction, while the optimized geometries of the species involved in this profile are presented in Figure 2. These results are in a good agreement with the Herbst and Woon.¹ In their work this authors display the potential energy surface and feasible exit channel to C₄H₂. In their work, Herbst and Woon argue that the potential surface is strongly attractive in nature and leads to a deep potential minimum in which the C₂H reactant attaches itself to a carbon atom of the acetylene. According to the authors, there is no energetic barrier in the entrance channel between the reactants and the potential minimum, the structure of which is referred to as a complex and the dissociation of the complex to form products must occur over a minimal potential barrier

or saddle point, the corresponding structure of which is known as a transition state. After rising to the transition state energy, which occurs below the energy of the reactants, the potential surface of the reactants, the potential surface goes downward to form the

exothermic products, H and C₄H₂, the latter being the nonpolar diacetylene structure, HCCCC, rather than the carbene structure, H₂CCCC, which has been detected in the interstellar medium.¹

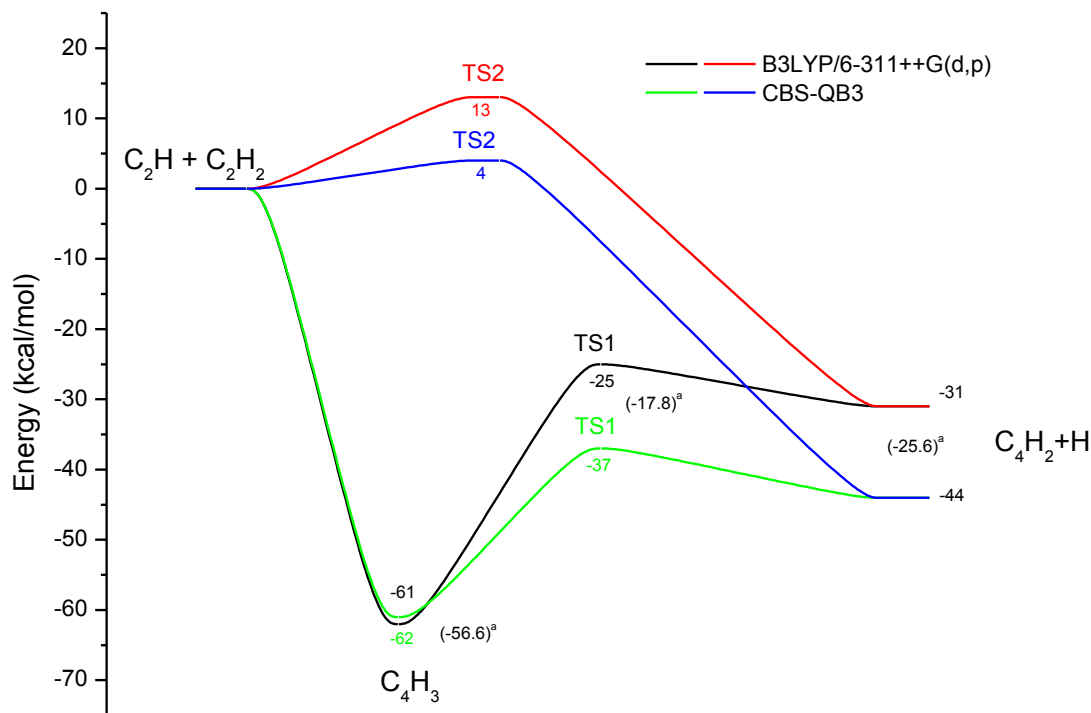


Figure 1. Potential energy diagram for decomposition of C₂H+C₂H₂ reaction at the B3LYP/6-311++G(d,p) and CBS-QB3, level. ^aZPE corrected values at RCCSD(T) in parents from Herbst and Woon¹

In Figure 1, we show the C₂H+C₂H₂ reaction with the following products: H + C₄H₂. For this product we have two possible pathways. The first candidate for this product is C₂H + C₂H₂ → C₄H₃ → TS1 → H + C₄H₂. In this pathway the C₄H₃ participates as reactant with energy of -61 kcal mol⁻¹(B3LYP) or -62 kcal mol⁻¹ (CBS-QB3). The other channel that forms the same product is C₂H + C₂H₂ → TS2 → H + C₄H₂. In both pathways the product participates with energy of -31 kcal mol⁻¹(B3LYP) or -44 kcal mol⁻¹ (CBS-QB3). In the CBS-QB3 method, the optimization of the geometry is carried out using B3LYP/6-311G(2d,d,p) level. However, the corrected

energy is calculated using a coupled cluster calculation with triple excitations for the highest level calculation. This explain the difference between B3LYP/6-311++G(d,p) and CBS-QB3 energies in the curves shown in Figure 1.

In Figure 3, we have the classical potential energy (V_{MEP}) and vibrationally adiabatic potential energy curve (V_{ZPE}). The V_{MEP} and V_{ZPE} along the minimum energy path (MEP) as a function of the reaction coordinate for the C₂H + C₂H₂ reaction for both PES are shown in Figure 3. One can see from these figures that V_{ZPE} curves are similar to V_{MEP} curves for both

PES. The reactant energy value is lower than the product energy value. Thus, this reaction is endothermic.

Table 1 shows the values of the frequencies and zero-point energy (ZPE) of

the reactant, transition states and products of species studied and they are also compared with the experimental and theoretical reference data.

Table 1. Vibrational wavenumbers (cm^{-1}) and zero-point energy –ZPE (kJ/mol) for the species involved in the reaction of $\text{C}_2\text{H} + \text{C}_2\text{H}_2$, calculated to B3LYP/6-311++G(d,p) and CBS-QB3 levels

Species	Vibrational wavenumbers (cm^{-1})		References	ZPE (kJ/mol)
	B3LYP/6-311++G(d,p)	CBS-QB3 (B3LYP/6-311G(2d,d,p))		
C_2H_2	643.9, 643.9, 769.2, 769.3 2062.1, 3425.0, 3527.5,	638.7, 638.6, 769.4, 769.4, 2070.1, 3426.1, 3528.7	612, 730, 1974, 3289, 3374 ²³	B3LYP 70.82 CBS-QB3 70.83
C_2H	293.6, 298.3, 2083.5, 3455.6	568.6, 1272.1, 1741.3, 3364.3	-	B3LYP 36.67 CBS-QB3 41.55
C_4H_3	214.5, 346.3, 511.5, 654.1, 689.5, 705.4, 847.5, 870.1, 989.1, 1264.4, 1618.5, 2192.9, 3097.9, 3242.5, 3475.9	212.5, 339.0, 510.9, 647.0, 682.9, 704.4, 851.4, 872.1, 991.2, 1265.7, 1623.1, 2199.5, 3096.3, 3240.4, 3476.9	199, 228, 489, 574, 611, 875, 934, 996, 1252, 1313, 1594, 2137, 3162, 3245, 3457 ¹	B3LYP 123.90 CBS-QB3 123.89
TS1	852.7i, 258.1, 259.6, 464.6, 536.4, 547.2, 629.6, 667.5, 670.7, 678.0, 915.5, 2034.1, 2244.1, 3459.5, 3473.7	855.7i, 255.9, 256.3, 468.3, 529.8, 544.0, 629.2, 663.3, 664.9, 671.9, 916.3, 2038.2, 2248.6, 3460.2, 3476.4	1109i, 206,224, 478, 533, 555,622, 665,894,949,124 5, 1949, 2177, 3425, 3456 ¹	B3LYP 100.72 CBS-QB3 100.63
TS2	1841.6i, 173.6, 271.2, 409.0, 625.0, 822.6, 845.1, 892.5, 940.2, 1184.8, 1602.3, 1771.6, 1870.3, 3195.5, 3236.7	1852.1i, 164.9, 268.0, 405.1, 628.3, 825.8, 846.6, 894.7, 939.1, 1185.9, 1605.9, 1773.6, 1872.5, 3195.3, 3236.7	-	B3LYP 106.71 CBS-QB3 106.70
C_4H_2	243.7, 243.7, 539.6, 539.7, 671.9, 671.9, 674.2, 674.2, 916.5, 2104.5, 2280.7, 3475.0, 3476.7	235.4, 235.4, 526.9, 526.9, 662.4, 662.3, 662.7, 662.7, 917.1, 2110.7, 2285.2, 3475.7, 3477.7	-	B3LYP 98.77 CBS-QB3 98.34

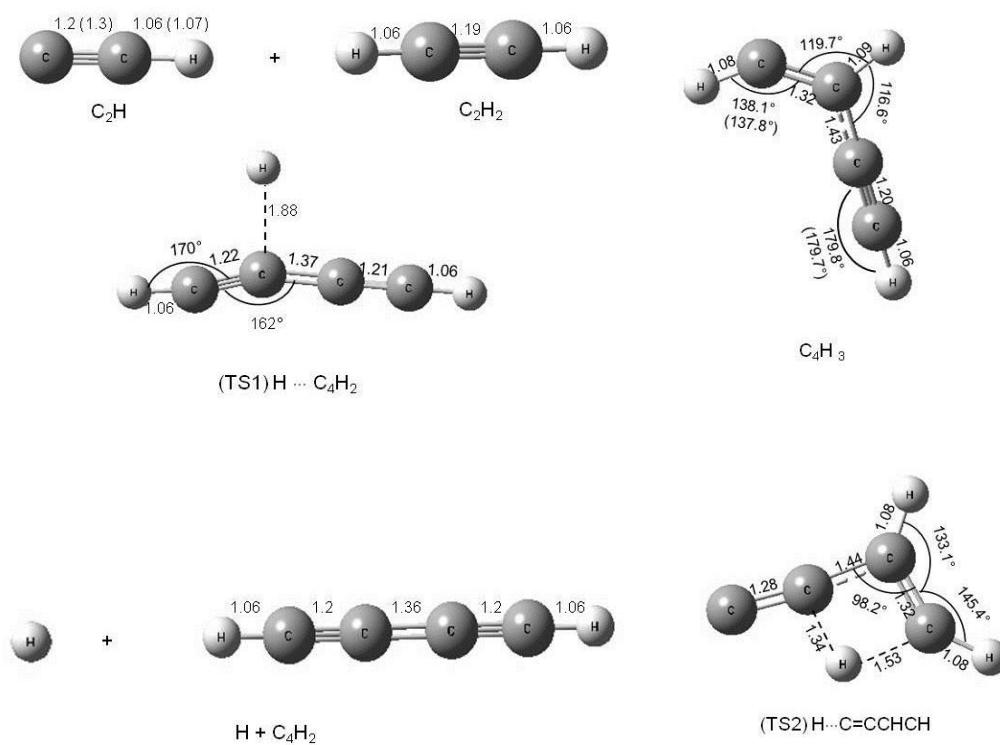


Figure 2. Optimized geometries for the species involved in the $C_2H + C_2H_2$ reaction pathways to B3LYP/6-311++G(d,p) level. The units for bond lengths and bond angles are Å and degrees, respectively

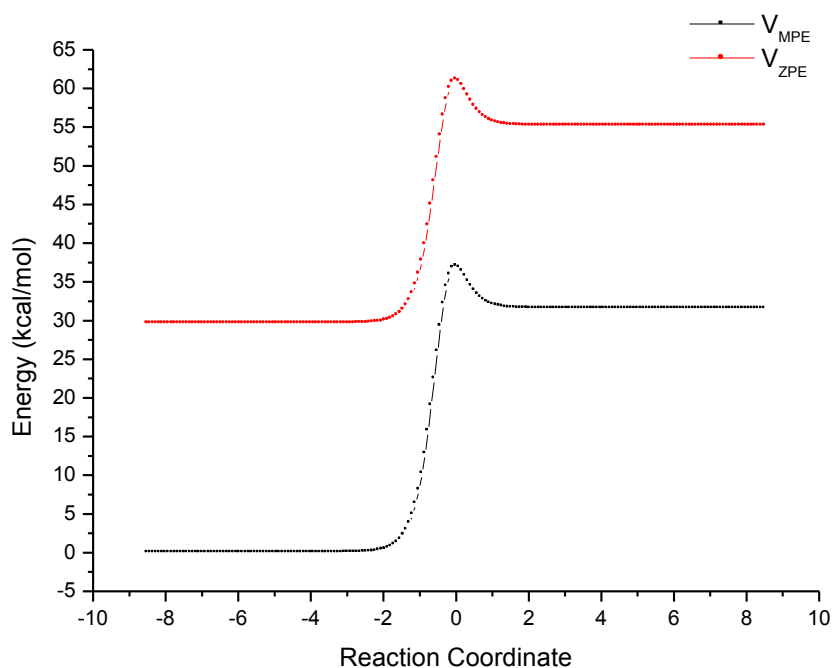


Figure 3. Classical potential energy curve (V_{MEP}) and vibrationally adiabatic potential energy curve (V_{ZPE}), as function of the reaction coordinate, calculated to B3LYP/6-311++G(d,p) level.

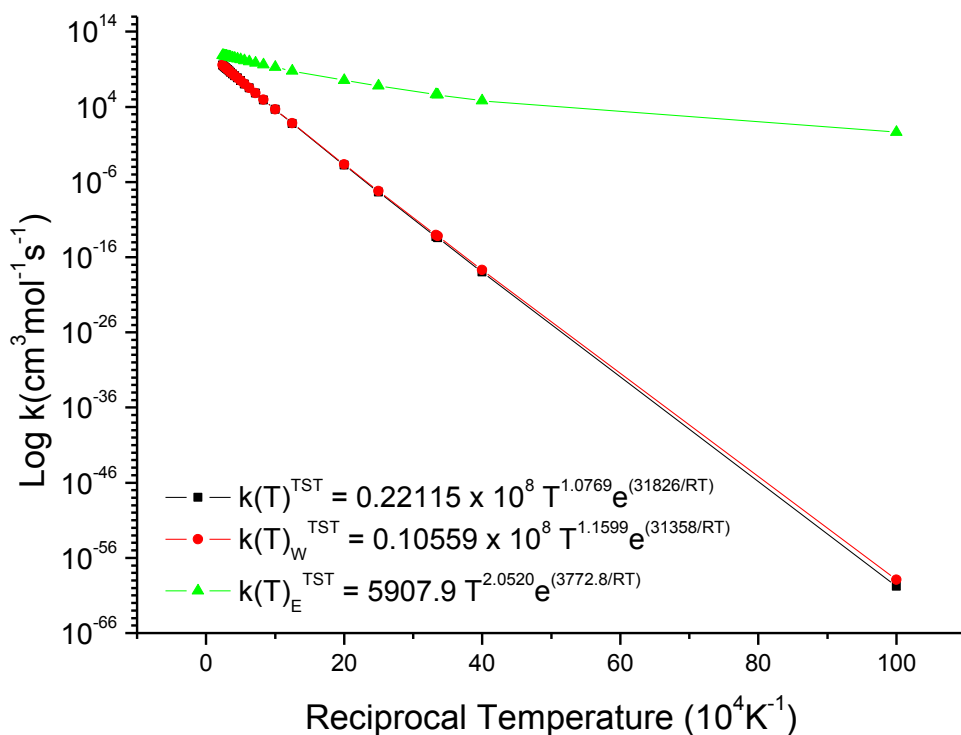


Figure 4. Arrhenius plot of against the reciprocal temperature in the range of 100–4200 K for reaction $C_2H + C_2H_2 \rightarrow C_4H_3 \rightarrow TS1 \rightarrow H + C_4H_2$, calculated to B3LYP/6-311++G(d,p) level

3.2. Rate Constants

To determine the reaction rate of the $C_2H + C_2H_2$ system we using a simple program that considering conventional TST method²⁴ with the Wigner²⁴⁻²⁶ transmission coefficient that is used to account for the tunneling effect along the reaction coordinate. The other tunneling correction used in our work is based one-dimensional Eckart potential barrier. The TST was developed during the 1930s and has since formed a framework for much of the discussion of rate processes. The model determines the rate constants based on an interaction potential between reactant and products with a statistical representation of the dynamics. In addition to the Born–

Oppenheimer approximation, it uses three more assumptions: there is a surface in phase space that divides into a reactant region and a product region; the reactant equilibrium is assumed to maintain a Boltzmann energy distribution, and the transition state or activated complex is assumed to have a Boltzmann energy distribution corresponding to the temperature of the reacting system.²⁴

To calculate rate constant with the CBS-QB3 method, the geometry is optimized in B3LYP/6-311G(2d,d,p) level. How this base set in CBS-QB3 is less accurate in compared with the base set used by us, we decided calculate the reaction rate only in B3LYP/6-311++G(d,p).

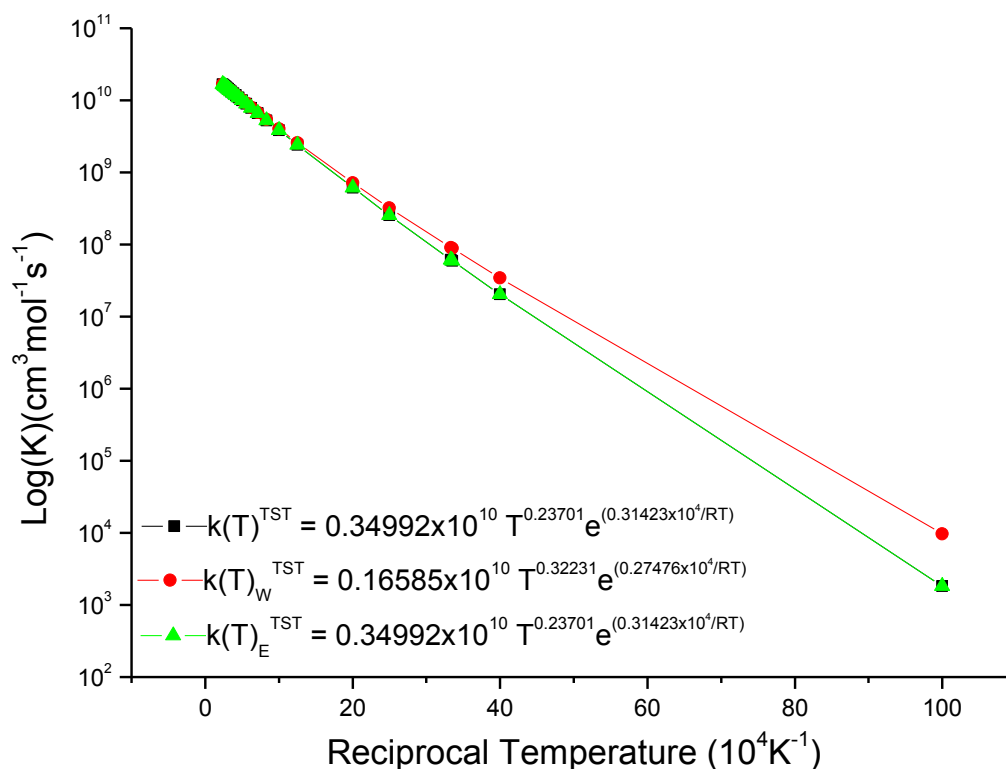


Figure 5. Arrhenius plot of against the reciprocal temperature in the range of 100–4200 K for reaction $C_2H + C_2H_2 \rightarrow TS2 \rightarrow H + C_4H_2$ calculated to B3LYP/6-311++G(d,p) level

In Figures 4 and 5 we show our results for rate constants of the two pathways of the reaction $C_2H + C_2H_2$. Since the apparent barrier is positive (see Figure 1), the reaction rate increases as the temperature increases. In Table 3 we show our results for reaction rate for: $C_2H + C_2H_2 \rightarrow C_4H_3 \rightarrow TS1 \rightarrow H + C_4H_2$ (pathway1) and $C_2H + C_2H_2 \rightarrow TS2 \rightarrow H + C_4H_2$ (pathway 2), both to the temperature of 300 K and 2400 K. These results show that the rate constants for the pathway 1 at 300 K present a significant discrepancy when compared with the values of k shown in reference (Table 3). For the high temperature of 2400 K we have an improvement for the reaction rates but still far of the reference values shown in Table 3. The reaction rates for the pathway 2 at 300 K and 2400 K are very similar values in both temperatures. These results show that at low and high temperatures we did not have an improvement in the possibility of occurrence for this reaction. 4×10^{-10} [Herbst]^{b,1}

Herbst and Woon,¹ in their work, found a considerable discrepancy for k (rate constant) involving the same reaction in compared with the value experimental obtained by Baulch *et. al.*²⁷ and they explained that this discrepancy is due to the calculated rate coefficient at room temperature is undoubtedly too large because the centrifugal barrier occurs at a sufficiently small distance, that the isotropic approximation is not justified. Neglecting the induction portion of the long-range potential, the minimum separation between ethynyl radical (C_2H) and acetylene, at which the centrifugal barrier occurs. For the new pathway $C_2H + C_2H_2 \rightarrow TS2 \rightarrow H + C_4H_2$ our results predict a very large barrier occurs and this has a considerable impact on the calculation of the reaction rate. In the literature we not found experimental or theoretical results for comparison with this new pathway.

Table 3. Second order rate constants calculated for the $C_2H + C_2H_2 \rightarrow C_4H_3 \rightarrow TS1 \rightarrow H + C_4H_2$ reaction (Pathway1) and $C_2H + C_2H_2 \rightarrow TS2 \rightarrow H + C_4H_2$ (pathway 2) at 300 K and 2400 K

T(K)	$k [cm^3.s^{-1}]^a$ – Path 1	$k [cm^3.s^{-1}]^a$ – Path 2	References [$cm^3.s^{-1}$]
300	$8.48 \times 10^{-38} (k^{TST})$	$1.02 \times 10^{-16} (k^{TST})$	4×10^{-10} [Herbst] ^{b,1}
	$1.44 \times 10^{-37} (k_W^{TST})$	$1.50 \times 10^{-16} (k_W^{TST})$	$(5.0 \pm 0.3) \times 10^{-11}$ [Baulch] ^{c,27}
2400	$7.16 \times 10^{-19} (k_E^{TST})$	$4.74 \times 10^{-14} (k_E^{TST})$	
	$2.22 \times 10^{-16} (k^{TST})$	$1.95 \times 10^{-14} (k^{TST})$	
	$2.24 \times 10^{-16} (k_W^{TST})$	$1.97 \times 10^{-14} (k_W^{TST})$	
	$4.76 \times 10^{-14} (k_E^{TST})$	$1.95 \times 10^{-14} (k_E^{TST})$	

^a Current results

^b From the *Herbst et. al.* $10 < T < 300$ K

^c From the *Baulch et. al.* $300 < T < 2700$ K

4. Conclusions

In this work, the $C_2H + C_2H_2$ reaction potential energy profiles were determined based on the geometrical optimization, frequency and energy calculations at the B3LYP/6-311++g(d,p) level. Our work predicted one new pathway for the $C_2H + C_2H_2$ reaction given by $C_2H + C_2H_2 \rightarrow TS2 \rightarrow H + C_4H_2$ (pathway 2) the other pathway to same product is $C_2H + C_2H_2 \rightarrow C_4H_3 \rightarrow TS1 \rightarrow H + C_4H_2$ (pathway 1) is predicted by Herbst and Woon¹. Our results for this pathway 1 show a good agreement for energies (with ZPE correction) of the complex reactant and product: -61 kcal/mol, -31 kcal/mol to

B3LYP/6-311++G(d,p) and -62 kcal/mol, -44 kcal/mol to CBS-QB3, respectively; in comparison with the results found by Herbst and Woon¹ with RCCSD(T) method: complex reactant (-56.6 kcal/mol with ZPE correction) and product (-25.6 kcal/mol without ZPE correction). For pathway 2 ($C_2H + C_2H_2 \rightarrow TS2 \rightarrow H + C_4H_2$) show the barrier of the 13 kcal/mol and 4 kcal/mol to B3LYP/6-311++G(d,p) and CBS-QB3, respectively, with ZPE corrections.

About the rate constants, we obtained result for $C_2H + C_2H_2 \rightarrow C_4H_3 \rightarrow TS1 \rightarrow H + C_4H_2$ that presented a discrepancy with some experiments and theoretical values at 300 K. With respect to accurate calculation of the rate coefficient for $C_2H + C_2H_2$ at temperature

in the range 50-300 K, Herbst and Woon argue that the intermediate-range forces that are anisotropic in nature need to be considered, the variational transition state formulation is a useful approach in the temperature range needed, although it requires significantly more ab initio information than the phase-space approach. It is expected that such a theory would show the rate coefficient for $C_2H + C_2H_2$ to reach a maximum somewhere in the vicinity of 50 – 100 K and then to decline slowly as the temperature reaches room temperature.^{28,29} The pathway 2 showed us a high rate constant. This result is an indicative that the pathway 2 has a large barrier that difficult the reaction in this way. The large rate coefficient calculated at low temperatures for the reaction between C_2H and C_2H_2 is probably not unique for radical hydrocarbon-stable hydrocarbon reactions.

Acknowledgements

The authors acknowledge the Instituto de Educação, Ciência e Tecnologia do Goiás - IFG and Universidade de Brasília – UnB.

References

- Herbst, E.; Woon, D. E. The Rate of the Reaction between C_2H and C_2H_2 at interstellar Temperatures. *The Astrophysical Journal* **1997**, *489*, 109. [CrossRef]
- Stephens, J. W.; Hall, Jeffrey L.; Soka, H.; Yan, W.-B.; Curl, R. F.; Glass, G. P. Rate constant measurements of reactions of ethynyl radical with hydrogen, oxygen, acetylene and nitric oxide using color center laser kinetic spectroscopy. *The Journal of Physical Chemistry* **1987**, *91*, 5140. [CrossRef]
- Woon, D. E. Modeling chemical growth processes in Titan's atmosphere: Theoretical rates for reactions between benzene and the ethynyl (C_2H) and cyano (CN) radicals at low temperature and pressure. *Chemical Physics* **2006**, *331*, 67. [CrossRef]
- Landera, A.; Krishtal, S. P.; Kislov, V. V.; Mebel, A. M.; Kaiser, R. I. Theoretical study of the C_6H_3 potential energy surface and rate constants and product branching ratios of the $C_2H(^2\Sigma^+) + C_4H_2(^1\Sigma_g^+)$ and $C_4H(^2\Sigma^+) + C_2H_2(^1\Sigma_g^+)$ reactions. *The Journal of Chemical Physics* **2008**, *128*, 214301. [CrossRef]
- Woon, D. E.; Herbst R. The Rate of the Reaction between CN and C_2H_2 at Interstellar Temperatures. *The Astrophysical Journal* **1997**, *477*, 204. [CrossRef]
- Chastaing, D.; James, P. L. ; Sims, I. R.; Smith, I. W. M. Neutral-neutral reactions at the temperatures of interstellar clouds Rate coefficients for reactions of C_2H radicals with O_2 , C_2H_2 , C_2H_4 and C_3H_6 down to 15 K. *Faraday Discussions* **1998**, *109*, 165. [CrossRef]
- Fukuzawa, K.; Osamura Y. Molecular Orbital Study of Neutral-Neutral Reactions concerning HC_3N Formation in Interstellar Space. *The Astrophysical Journal* **1997**, *489*, 113. [CrossRef]
- Kovács, T.; Blitz, M. A.; Seakins, P. W. H-Atom Yields from the Photolysis of Acetylene and from the Reaction of C_2H with H_2 , C_2H_2 , and C_2H_4 . *The Journal of Physical Chemistry A* **2010**, *114*, 4735. [CrossRef]
- Ridgway, S. T. Jupiter: Identification of Ethane and Acetylene. *The Astrophysical Journal* **1974**, *187*, L41. [CrossRef]
- Moos, H. W.; Clarke, J. T. Detection of Acetylene in the Saturnian Atmosphere, using the IUE Satellite. *The Astrophysical Journal* **1979**, *229*, L107. [CrossRef]
- Homann, K. H.; Wagner, H. G. Chemistry of carbon formation in flames. *Proceedings The Royal Society A* **1968**, *307*, 141. [CrossRef]
- Tucker, K. D.; Kutner, M. L.; Thaddeus, P. The ethynyl radical C_2H – A new Interstellar Molecule. *The Astrophysical Journal* **1974**, *193*, L115. [CrossRef]
- Strobel, D. F. Chemistry and evolution of Titan's atmosphere. *Planetary and Space Science* **1982**, *30*, 839. [CrossRef]
- Laufer, A. H.; Bass, A. M. Photochemistry of acetylene. Bimolecular rate constant for the formation of butadiyne and reactions of

ethynyl radicals. *The Journal of Physical Chemistry* **1979**, *83*, 310. [CrossRef]

¹⁵ Laufer, A. H. Reactions of ethynyl radicals. Rate constants with methane, ethane, and ethane-d₆. *The Journal of Physical Chemistry* **1981**, *85*, 3828. [CrossRef]

¹⁶ Laufer, A. H.; Lechleider, R. Reaction of ethynyl radicals with oxygen. Rate constant for formation of carbon monoxide. *The Journal of Physical Chemistry* **1984**, *88*, 66. [CrossRef]

¹⁷ Becke, A.D. Density-functional thermochemistry. III. The role of exact exchange. *The Journal of Chemical Physics* **1993**, *98*, 5648. [CrossRef]

¹⁸ Montgomery, J. A.; Frisch, M. J.; Ochterski, J. W.; Petersson, G. A. A complete basis set model chemistry. VI. Use of density functional geometries and frequencies. *The Journal of Chemical Physics* **1999**, *110*, 2822. [CrossRef]

¹⁹ M^o, O.; Y^añez, M.; Elguero, J. Cooperative (nonpairwise) effects in water trimers: An *ab initio* molecular orbital study. *The Journal of Chemical Physics* **1992**, *97*, 6628. [CrossRef]

²⁰ Raghavachari, K.; Trucks, G. W.; Pople, J. A.; Head-Gordon, M. fifth-order perturbation comparison of electron correlation theories. *Chemical Physics Letters* **1989**, *157*, 479. [CrossRef]

²¹ Frisch, M. J.; Trucks, G. W.; Schlegel, H. B.; Scuseria, G. E.; Robb, M. A.; Cheeseman, J. R.; Scalmani, G.; Barone, V.; Mennucci, B.; Petersson, G. A.; Nakatsuji, H.; Caricato, M.; Li, X.; Hratchian, H. P.; Izmaylov, A. F.; Bloino, J.; Zheng, G.; Sonnenberg, J. L.; Hada, M.; Ehara, M.; Toyota, K.; Fukuda, R.; Hasegawa, J.; Ishida, M.; Nakajima, T.; Honda, Y.; Kitao, O.; Nakai, H.; Vreven, T.; Montgomery, J. A., Jr.; Peralta, J. E.; Ogliaro, F.; Bearpark, M.; Heyd, J. J.; Brothers, E.; Kudin, K. N.; Staroverov, V. N.; Kobayashi, R.; Normand, J.; Raghavachari, K.; Rendell, A.; Burant, J. C.; Iyengar, S. S.; Tomasi, J.; Cossi, M.; Rega, N.; Millam, J. M.; Klene, M.; Knox, J. E.; Cross, J. B.; Bakken, V.; Adamo, C.; Jaramillo, J.;

Gomperts, R.; Stratmann, R. E.; Yazyev, O.; Austin, A. J.; Cammi, R.; Pomelli, C.; Ochterski, J. W.; Martin, R. L.; Morokuma, K.; Zakrzewski, V. G.; Voth, G. A.; Salvador, P.; Dannenberg, J. J.; Dapprich, S.; Daniels, A. D.; Farkas, Ö.; Foresman, J. B.; Ortiz, J. V.; Cioslowski, J.; Fox, D. J. Gaussian, Inc., Wallingford CT, 2009. [Link]

²² Pokon, E. K.; Liptak, M. D.; Feldgus, S.; Shields, G. C. Comparison of CBS-QB3, CBS-APNO, and G3 Predictions of Gas Phase Deprotonation Data. *The Journal of Physical Chemistry A* **2001**, *105*, 10483. [CrossRef]

²³ NIST Livro de Química na Web. Base de dados de Referência padrão do NIST número 69. Disponível em: <<http://webbook.nist.gov/chemistry/>>. Acesso em: 14 abril 2015.

²⁴ Truhlar, D. G.; Isaacson, A. D.; Garrett, B. C.; *Generalized Transition State Theory, Theory of Chemical Reaction Dynamics*, Vol 4; CRC Press: Boca Raton, FL, 1985; p 65.

²⁵ Henon, E.; Bohr, F. Comparative *ab initio* MO investigation on the reactivity of the three NH(a¹Δ), NH(X³Σ⁻) and NH₂(X²B₁) radical species in their bimolecular abstraction gas-phase reaction with the HN₃ molecule. *Journal of Molecular Structure: THEOCHEM* **2000**, *531*, 283. [CrossRef]

²⁶ Rapp, D.; *Statistic Mechanics*, Holt, Rinehart and Winston, Inc: New York, 1972.

²⁷ Baulch, D. L., Cobos, C. J.; Cox, R. A.; Esser, C.; Frank, P.; Just, Th.; Kerr, J. A.; Pilling, M. J.; Troe, J.; Walker, R. W.; Warnatz, J. Evaluated Kinetic Data for Combustion Modeling. *Journal of Physical and Chemical Reference Data* **1992**, *21*, 411. [CrossRef]

²⁸ Klippenstein, S. J., Kim, Y.-W. Variational statistical study of the CN+O₂ reaction employing *ab initio* determined properties for the transition state. *The Journal of Chemical Physics* **1993**, *99*, 5790. [CrossRef]

²⁹ Herbst, E. In *Atomic, Molecular, and Optical Physics Reference Book*; Drake, G., ed.; AIP: New York, 429, 1996.